Ozone decrease observed in the upper atmosphere following the May 11th 2024 ~~*Mother's day*~~ *Mother's Day* solar storm.

Alexandre Winant[1, 2], Viviane Pierrard[1, 2], and Edith Botek[1]

[1]Solar Wind, Space Physics and Solar-Terrestrial Center of Excellence, Royal Belgian Institute for Space Aeronomy (BIRA-IASB), Avenue Circulaire 3, Brussels, Belgium

[2]Center for Space Radiations (CSR), Earth and Life Institute, Climate Sciences ELI-C, Université Catholique de Louvain (UCLouvain), Louvain-la-Neuve, Belgium

Correspondence: Alexandre Winant (alexandre.winant@aeronomie.be)

Abstract. On May 11th 2024, a succession of coronal mass ejections that merged together struck the Earth and induced large scale perturbations in the magnetosphere. During this event, satellite observations showed a large solar energetic ~~proton~~ particle (SEP) event associated to an extreme geomagnetic storm. At the same time, satellite observations of atmospheric ozone have been performed by the AURA/MLS instrument. In this work, we present the first observations of the effect of the storm of May and the following SEP of June 8th on ozone concentration throughout the atmosphere. Observations of the MLS show that the event of May ~~lead~~ led to stronger depletion of ~~O_3 in the upper part of the atmosphere~~ O_3 in the mesosphere and lower thermosphere (MLT) than in June. This difference is explained by the type of particle precipitation that occurred during the two events, with both protons and electrons in May and only protons in June. Neither event caused ozone depletion in the stratosphere while strong decreases are observed in the mesosphere. In May, mesospheric ozone depletion is observed during 18 days and reaches a maximum of 60%. In addition, the storm of May also caused a noticeable decrease in ozone concentration (up to 20%) at altitudes above 90 km.

1 Introduction

While solar cycle 25 is approaching its maximum activity (predicted in 2025), the probability of strong solar events is also expected to rise. Both the frequency and the intensity of solar events increase around the maximum and the declining phase of the cycle although the strongest event take place during the descending phase. The year 2024 is located at the end of the ascending phase of cycle 25, making it prone to be subjected to large perturbations of solar origin (Abe et al. (2023)). On the 11th of May 2024, an extreme geomagnetic storm associated with a large Forbush ~~deacrease~~ decrease in galactic cosmic rays were observed on the ground ~~Mavromichalaki et al. (2024)~~(Mavromichalaki et al. (2024)). The cause of the extreme event of May 2024 ~~is~~ was a succession of ~~CMEs (Coronal Mass Ejections~~coronal mass ejections (CMEs) that merged together and simultaneously struck the Earth, which ~~lead~~ led to an extreme perturbation of the magnetosphere ~~Kwak et al. (2024)~~ (Kwak et al. (2024)). Moreover, a large Solar Energetic Particle (SEP) event was observed in the vicinity of the Earth by space borne particle detectors ~~Pierrard et al. (2024)~~(Pierrard et al. (2024)). This geomagnetic storm ~~is~~ was the largest observed in more than 20 years, reaching a minimum Disturbed Storm time index $Dst_{min} = -412$ nT and a maximum Bartels planetary index of geomagnetic activity $Kp_{max} = 9$. The last observation of an event with a similar magnitude dates back to the famous 2003 Halloween geomagnetic storm with a minimum $Dst_{min} around -400$ nT. Dst_{min} around -400 nT. A recent study by (Elvidge and Themens (2025)) shows that this storm was a 1 in 12.5 year event in term of magnitude and a 1 in 41 year event in term of duration. Moreover, this event was categorized as the sixth strongest storm observed since 1957 (Hayakawa et al. (2025)). The geomagnetic storm of May 11^{th} was responsible for large variations in the radiation belts of the Earth, in which where a temporary 4 belts structure was observed at low Earth orbit Pierrard et al. (2024). On the 8^{th} of June 2024, 27 days after the extreme event of May , another SEP eventhas been observed near Earth. (Pierrard et al. (2024)). Observations of major disturbances in the ionosphere have also been reported all over the globe (Themens et al. (2024); Singh et al. (2024); Huang et al. (2024)). In addition, enhanced Joule heating caused by the storm of May lead to sharp rise in thermospheric densities for one day before recovering the day after due to cooling from increased NO concentration (Ranjan et al. (2024)). At lower altitudes in the thermosphere, measurement from the GOLD instrument showed global changes in composition and temperature following the event, with temperature increasing up to 1400 K at high latitudes at 160 km (Evans et al. (2024)). Global increase of temperature in the mesosphere and lower thermosphere were also reported by (Liu et al. (2025)).

Enhanced geomagnetic activity also leads to increased energetic electron precipitation (EEP) in the atmosphere at high latitude which latitudes. They mainly consist of auroral electrons originating from the magnetotail and radiation belt electrons in the bounce loss cone. Energetic protons of solar origin also precipitate in the atmosphere as they are guided toward high latitudes by the Earth''s magnetic field. As they penetrate into the atmosphere, energetic particles interact with the constituents of the atmosphere inducing their excitation, dissociation and ionization Sinnhuber et al. (2012); Mironova et al. (2015). Following the interaction of the atmosphere with the energetic precipitating particles (EPP) , complex chains of chemical reactions take place in different layers of the atmosphere which can lead to the formation of odd hydrogen $(HO_x = H + HO + HO_2)$ and odd nitrogen $(NO_x = N + NO + NO_2)$ via ion-neutral chemistry Verronen and Lehmann (2013). NO_x (Sinnhuber et al. (2012); Mironov). Subsequent neutral-ion chemistry leads to the to the formation of odd hydrogen ($HO_x = H + HO + HO_2$) and odd nitrogen ($NO_x = N + NO + NO_2$) (Solomon et al. (1981, 1982); Turunen et al. (2009); Rozanov et al. (2012); Verronen and Lehmann (2013)). Increased HOx productions by SEP mainly occur in the mesosphere and upper stratosphere and is expected to efficiently destroy ozone through a well known chain of catalytic reactions (Verronen et al. (2006); Grenfell et al. (2006)). In addition to SEP, energetic electron precipitation (EEP) from the radiation belts have been found to also have a significant influence on HO_x production in the mesosphere (Verronen et al. (2011); Andersson et al. (2012)). At these altitudes, HO_x has a short lifetime of a few hours (Pickett et al. (2006)) and its impact on ozone is fast but also of short duration (a few days) (Smith et al. (2018b)). During the SEP events of January 2005 and December 2006, both satellite observations and simulations have shown a temporary destruction of mesospheric ozone caused by boosted concentration of HO_x. (Verronen et al. (2006); Seppälä et al. (2006); Sofiev). Similarly, increased EEP can be responsible for depleting the ozone between 60 km and 80 km by 90% on short time scales (Andersson et al. (2014)). Nitrogen oxides NOx are mainly produced in the upper part of the atmosphere, in the mesosphere (50 to 90 km) and lower thermosphere, where their production rate in the lower thermosphere (90 to 100 km), where its concentration is increased by EPP Sætre et al. (2004). Those species are (SEP + EEP) (Sætre et al. (2004); Turunen et al. (2009)

). Odd nitrogen is long lived in the atmosphere , especially during polar winter. In the presence of the polar vortex, NO_x produced in the mesosphere and lower thermosphere (MLT) region can be efficiently transported downward at those altitudes in the absence of sun light. During the polar winter, NO_x can be accumulated and transported downward without significant losses to the stratosphere (10 to 50 km in average) and by the Brewer–Dobson circulation inside the polar vortex (Funke et al. (2005)) and efficiently deplete the ozone in this region of the atmosphere Randall et al. (2007); Funke et al. (2014, 2016). Mesospheric HO_x levels have been observed to correlate with the precipitation of electrons from the radiation belts Verronen et al. (2011); Andersson et . HO_x are short lived, thus their response to EPP is localized in space and time, where and when ionization is increased Mironova et al. (2015). HO_x and NO_x contribute to the depletion of ozone through catalytic reactions Lary (1997). Thus, the net result of EPP is to contribute to decrease the ozone concentration in the atmosphere and can have repercussion on climate Rozanov et al. (2012); Seppälä et al. (2014).

The response of ozone in the atmosphere to EPP (of both protons and electrons)has been extensively studied over the years. Energetic Electron Precipitations (EEP) have been found to have a significant influence on O_3 in the mesosphere between 60 km and 80 km, where it could be depleted by 90% on a short term scale Andersson et al. (2012). (Lary (1997); Jackman et al. (2001); Randall et). Because they have the possibility to ionize lower layers in the atmosphere, energetic solar protons may contribute to deplete ozone in the upper stratosphere. However, strong evidence of SEP directly depleting stratospheric ozone are scarce. In the study of Jia et al. (2020)(Jia et al. (2020)), changes of ozone were observed by MLS after SEPs between 2004 up to 2020. Although clear ozone depletion can be observed at high altitudes following multiple SEPs, only one event was found to have an effect on the stratospheric ozone.

In this paper, we use observations from the Microwave Limb Sounder (MLS) to investigate and provide a first report of the effect of the extreme solar and geomagnetic event of May as well as the following SEP of June on atmospheric ozone in the polar regions.

2 Data and methods

2.1 Ozone observations from AURA/MLS

The Microwave Limb Sounder (MLS) as part of the Earth Observing System (EOS) Evans and Greer (2000) (Evans and Greer (2000)) was launched in 2004 onboard the NASA satellite AURA on quasi-polar sun-synchronous orbit at 705 km of altitude. This instrument measures thermal radiation from Earth's atmosphere retrieving vertical profiles of the temperature and trace gases by scanning Earth's limb in the plane of its orbit. In this work, we mainly use ozone profiles from the MLS that are derived from radiances measured by the 240 GHz radiometer. More specifically, we use the latest version v5.0 of the MLS data product (Schwartz (2021)) with a spatial coverage ranging from -82° to 82° and that has an increased vertical range compared to previous versions. With v5.0, ozone observations in the upper mesosphere are available for scientific studies. In this work, we have applied all recommendations regarding data screening provided in the *MLS Level 2 Version 5 Quality Document* that can be found at (https://mls.jpl.nasa.gov/data/v5-0_data_quality_document.pdf). Moreover, we only use high latitude observations, comprised between 60° and 9082° in both hemispheres and then perform daily averages which are necessary for the highest altitudes in the mesosphere. (Level 2 ozone data from MLS are available at https://disc.gsfc.nasa.gov/datasets/ML2O3_005/summary, last accessed on 29/10/2024)

2.2 In situ observations of energetic particles

For the solar proton fluxes, we use the observations from the Geostationary Operational Environmental Satellite (GOES) which is fitted with the Energetic Proton, Electron, and Alpha Detector (EPEAD). This instrument measures the flux of protons in 7 energy channels spanning from 0.74 to 900 MeV. The data used in this work consists of integral proton fluxes with energies > 10 MeV, > 30 MeV, > 100 MeV which have a resolution of 5 minutes. (Data are accessible at: https://lasp.colorado.edu/space-weather-portal/, last accessed on 29/10/2024)

In order to determine when energetic electrons from the radiation belts precipitate into the atmosphere, we use the POES/MEPED detector on the MetOP satellite. The MEPED instrument is composed of two pairs of directional detectors. The first pair is dedicated to the measurement of protons with energies ranging from 30 keV to 200 MeV. The second pair of detectors measures the fluxes of electrons of energies between 30 keV to 2500 keV in 3 integral channels. For a given type of particles, the two telescopes are arranged perpendicular to one another and are referred to as the 0° telescope and the 90° telescope. On ~~MetOp~~MEPED, the 0° telescope points directly to the zenith and the 90° telescope points to the antiram direction (i.e., opposite to the velocity vector of the spacecraft). At high latitudes, the 0° telescope mainly measures particles in the Bounce Loss Cone (BLC) and thus precipitating into the atmosphere.

2.3 Assessing the impact on ozone and temperature

The ~~main strategy~~ first approach to quantify the effect of the May and June events on ozone through the atmosphere is taking the average profile of ozone before the event (quiet ozone profile), and computing its difference relative to the daily profiles for the rest of the month. The quiet period consists of the five daily profiles observed before either the maximum proton flux observed by GOES or the minimum in the Dst index. Those profiles are then averaged on time to provide the quiet conditions.

~~Another~~ The second approach used in this work is to first compute the long term trend in the profiles observed by MLS. In order to do so, a lowess (locally weighted scatter plot smoothing) algorithm, introduced by (Cleveland (1979)) was applied to the daily profiles from MLS spanning from January 1^{st} 2024 to June 30^{th}. In practice, we use the *lowess* function from the *Statsmodel* python library with a value of frac = 0.25. With the results of the lowess algorithm, the daily detrended profiles are computed, revealing only the short term variations which can then be compared to daily averaged geomagnetic activity.

3 Results

Figure 1 shows the daily averaged MLS ozone profiles at high latitudes from the beginning of 2024 to June 30^{th}. The top panel corresponds to the high southern latitudes comprised between -60° and ~~-90~~ -82° of latitude and the middle panel corresponds to the northern latitudes comprised between 60° and ~~90~~82°. The last panel of this figure shows the geomagnetic activity for the period, displaying both the Dst and Kp indices. The bottom panel of the figure indicates that during the beginning of the year, the geomagnetic activity is very low, with the Kp index barely exceeding 4. It is only in March that a noticeable geomagnetic storm was recorded in both Dst and Kp. The next big event took place in mid April with a Dst below -100 nT and a Kp of 7. Form this point onward, these indices show that the magnetosphere was repeatedly disrupted by intense storms until the extreme event of May 11 occurred with a minimum Dst value never seen in 20 years of - 412 nT and a Kp of 9. During the recovery phase of this major event, some other intense events took place and the Dst index remained quiet until the end of June.

All along this period, the AURA/MLS instrument continuously carried out measurements of ozone throughout the atmosphere. The first panel of Fig. 1 clearly illustrates the different ozone layers that exist in the atmosphere. The main ozone layer located in the stratosphere, the secondary layer in the upper mesosphere and lower thermosphere (MLT) region and finally the tertiary layer in the mesosphere where the maximum of ozone concentration is observed at around 75 km. Both the second and third ozone layers are subjected to very strong seasonal variations and are mostly depleted during local summer due to increased photodissociation (Marsh et al. (2001); Smith and Marsh (2005); Smith et al. (2018a)).

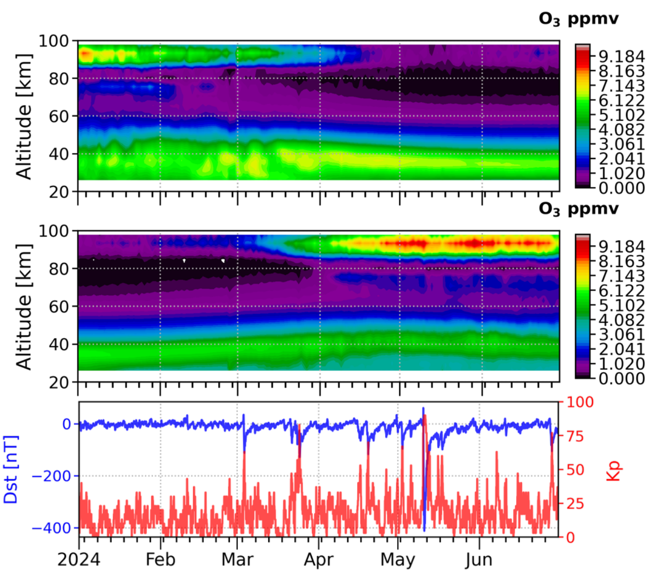

Figure 1. Daily averaged high latitude ([60°, ~~90~~82°]) ozone volume mixing ratio profiles from AURA/MLS as a function of time and altitude between January 1st and June 30st 2024. Top: northern hemisphere. Middle: southern hemisphere. Ozone volume mixing ration is expressed in parts per million by volume (ppmv). Bottom: Geomagnetic activity indices from the OMNI database between January 1^{st} and June 30^{th}. The Disturbed storm time (Dst) index is represented in blue and the planetary Kp index multiplied by 10 is displayed in red.

~~Thus in the northern hemisphere (NH), the ozone forming the~~ ozone in the secondary and tertiary layers gradually ~~gets depleted~~ diminishes from winter to summer~~, when the~~. During this period, mesospheric ozone is ~~completely~~ almost entirely removed from the atmosphere~~and the secondary layer ozone~~, decreasing from approximately 2.5 ppmv to below 1 ppmv, while the ozone in the secondary layer is reduced from ~~between~~ 7~~and~~ –8 ppmv to ~~between~~ 1~~and~~ –2 ppmv. In the southern hemisphere (SH) (middle panel of Fig. 1), the situation is reversed and ozone starts to accumulate in the mesosphere and the lower thermosphere.

In addition to the strong seasonal variations of ozone, the first and second panel of the figure clearly show that the ozone also experiences short term variations. Those variations on smaller time scales are not linked to geomagnetic storms illustrated by high peaks of geomagnetic activity in the bottom panel, in any of the ozone layers.

~~In order to observe a direct effect of solar energetic particles (SEP) in the stratospheric ozone layer, there must be a significant flux of protons with sufficient energy to ionize the stratosphere. Between January and May, some minor SEP events did occur but they had low fluxes and a soft spectrum which could not have impacted the stratospheric ozone. Soft protons can deposit their energy in the mesosphere, and some rapid decreases in O_3 happened in the NH after the particles injections at high altitudes, but not always. After the May 11 events, no ozone is left in the upper part of the atmosphere so that no ozone is lost further. Despite their hard spectrum and high fluxes, neither the May nor the June SEPs (see Fig. 2) have had any impact on the NH main ozone layer. One of the reasons might be due to the weakening of the polar vortex in the NH during late spring and summer.~~

In the SH, in the beginning of the year, no short term variation of ~~O_3~~ O_3 has been observed by MLS. However, the middle panel of Fig. 1 clearly shows a change of ozone concentration in the MLT region (at ~ 90 km) as well as in the mesosphere (at ~ 75 km) after the event of May. In the stratosphere, no sign of the event of May is discernible in the figure.

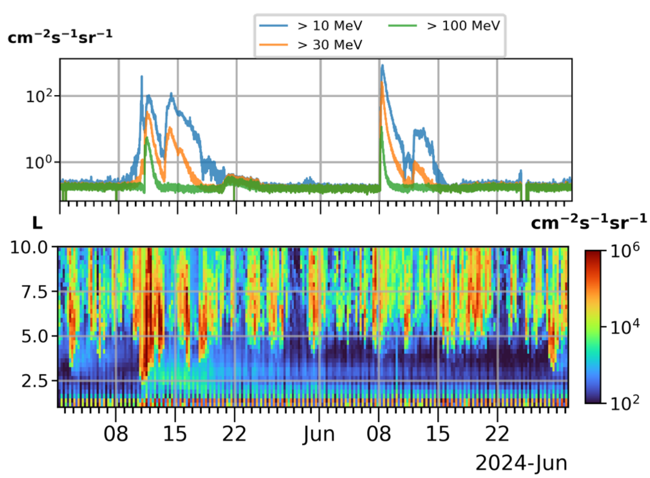

Figure 2. Top: Integral proton flux measured by GOES between May 01 and June 30, 2024 in three different energy channels. Bottom: Integral electron flux with energy >30 keV measured by POES 0° telescope and averaged in L-time bins [0.1L - 3h] displayed as a function of time and the McIlwain parameter over the the same time period.

The flux of ~~EPP~~ energetic precipitating particles (both protons and electrons) between May 1^{st} and June 30^{th} 2024 are presented ~~on the two~~ in both panels of Fig. 2. On the top, GOES observations of the integral proton fluxes with different energy threshold clearly show the two SEP events of May 11^{th} and June 8^{th}. This panel reveals that each of the two SEPs ~~have a~~

~~double peak in protons of > 10 MeV and > 30 MeV but not for protons with energies > 100 MeV~~ generates multiple peaks for protons of > 10 MeV and > 30 MeV due to repeated injections, wave-driven acceleration and relatively slow loss processes. In contrast, a single peak for >100 MeV fluxes is the result of the higher energy threshold for acceleration, faster loss mechanisms, and less efficient production mechanisms. The proton flux measured by GOES in June is very similar to the flux of May (see Fig. 2 top panel)~~, because they originate from the same region~~ . Both SEP were likely produced by the same active region at the surface of the Sun ~~and they are separated in time by one solar rotation~~ that was still active after one period of rotation (Jaswal et al. (2025)).

The second panel of Fig. 2 displays the integral flux of electrons with energies > 30 keV observed by the MEPED 0° telescope during the same period as GOES. In this case, the electron fluxes are presented as a function L, the McIlwain parameter (uniquely identifying Earth's magnetic shells) and time. Electron fluxes have been averaged on L-time bins of 0.1 L and 3 hours. At high latitudes and thus high L values, electrons observed by the 0° telescope are considered to precipitate into the atmosphere along the magnetic field lines ~~Rodger et al. (2010)~~(Rodger et al. (2010)). Unlike SEP events, electron precipitation in the atmosphere is a process that is constantly occurring but it is modulated by geomagnetic activity. Increased precipitation has been observed during the main phase of the geomagnetic storm of May 11 reaching the maximum flux of $\sim 1.2\ 10^6\ [\mathrm{cm}^2\mathrm{s\ sr}]^{-1}$ which is never attained again throughout the whole period.

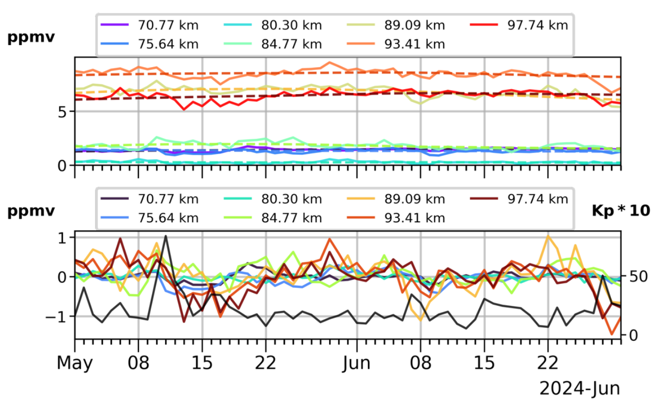

Figure 3. Top panel: The plain lines represent the daily averaged ozone vmr computed with AURA/MLS observations from May 1^{st} and June 30^{th} in the Southern hemisphere. The dashed lines are the computed long term trends in ozone vmr resulting from the lowess algorithm applied on the observations from January to June. Each color corresponds to an altitude level. Bottom panel: The daily detrended ozone vmr. Colors are the same as for the top panel. The black line represents the daily averaged Kp index multiplied by 10 computed from ~~omni~~ OMNI data.

As ozone concentration in the atmosphere is subject to seasonal variations and changes on longer time scales such as the solar cycle, we computed the long term variations in the MLS observation in order to extract only the ozone changes on small time scales between May 1^{st} and June 30^{th}. The long term trend in MLS observations was computed by applying the lowess algorithm on the daily ozone profiles. To ensure that the results of the algorithm could capture the seasonal variability, we used the data from January 1^{st} to June 30^{th} to compute the trend. The result of this data treatment is shown in the top panel of Fig. 3 together with the daily average ozone volume mixing ratio (vmr). Each color in the figure represents an altitude level ranging from 70 km to 97 km, covering the mesosphere and lower thermosphere. The bottom panel of the figure shows the detrended ozone vmr (i.e., daily ozone vmr minus the long term trend) at each altitude level. The black curve in this panel corresponds to the daily averaged Kp index(multiplied by 10) computed from the OMNI dataset. From this panel, it is clear that, following the peak in the Kp index which indicates the main phase of the geomagnetic storm of May 11^{th}, a rapid decrease in ozone vmr is observed by the MLS instrument for all altitudes between 70 km and 98 km. It then required 18 days for the ozone vmr to regain the pre-storm levels. In June, no major geomagnetic storm took place as shown by the daily Kp curve. However, the detrended ozone shows a noticeable decrease on the 7^{th} of June at 84 km. At higher altitudes, the decrease in ozone occurs on the 9^{th}, after the SEP event took place.

Figure 4 displays the results of the daily averaged measurements of O_3 (top left) and temperature (top right), as well as their relative difference in percentage between the pre-storm (i.e. quiet) ozone vmr (top panel), as well as temperature profile (bottom panel) level and all the daily profiles measured from the start of the period until the end of the month. The bottom left panel shows the results for the ozone and the bottom right shows the results for the temperature. The quiet period consists of the time averages of the daily profiles between May 5^{th} and May 9^{th}. The reason for not taking the profiles between the 6^{th} and 10*th* 10^{th} is that, even if the peak of the SEP flux and the main phase of the geomagnetic storm took place on May 11^{th}, the flux of lower energy protons (>10 MeV) has a first peak on the 10^{th} of May. So that May 10^{th} is neither considered as a quiet day nor is the peak of the event (when considering the proton spectrum and the geomagnetic activity). The top panel shows the relative difference computed with O_3 vmr and the bottom panel with temperature.

From the top panel of the figure, it is obvious that some ozone was lost during the period of interest. The vertical black dotted line indicates the day during which the daily averaged proton flux and geomagnetic activity are the highest (i.e. May 11^{th}). The Both left panels of Fig.4 show that the main ozone loss was observed takes place after the event in the tertiary layer at around 75 km. However, the day before, on May 10^{th}, the ozone vmr at those altitudes had already decreased by 20%. This premature decrease might be caused by the penetration of the low energy protons measured by GOES on that day, which efficiently deposit their energy around 70 km (see Fig. 1 of Sátori et al. (2016)(Sátori et al. (2016))). Two days after the main phase of the storm, ozone vmr at 80 km decreased by as much as 60%. This ozone deficit relative to pre-storm level remained until May 29^{th}, oscillating between 30 % to 50%. However, those values must be taken with caution since this altitude corresponds to the minimum between the tertiary and the secondary ozone layers, and the near zero values of ozone in this region can lead to large values of the relative difference. Moreover, after the event until May 17^th, the loss in ozone was observed in the tertiary layer between 70 km and 80 km. At those altitudes however, only around 75 km, in the tertiary layer, the decrease in ozone vmr was about 30%. At 70 km, 20% of the ozone is depleted from the mesosphereafter the storm. This ozone decrease is only observed down to 70 km and until May 18^{th}. In addition to the mesospheric ozone loss, in the MLT region above 90 km

Two days before the peak of the storm, the ozone vmr in the secondary layer did increase. This is visible in the detrended time series of Fig.3 and in the first panel of the Fig.4 in which the secondary layer slightly expanded. The largest increase was observed at 84 km of altitude, corresponding to the lower edge of the layer. This results in the positive values of the relative

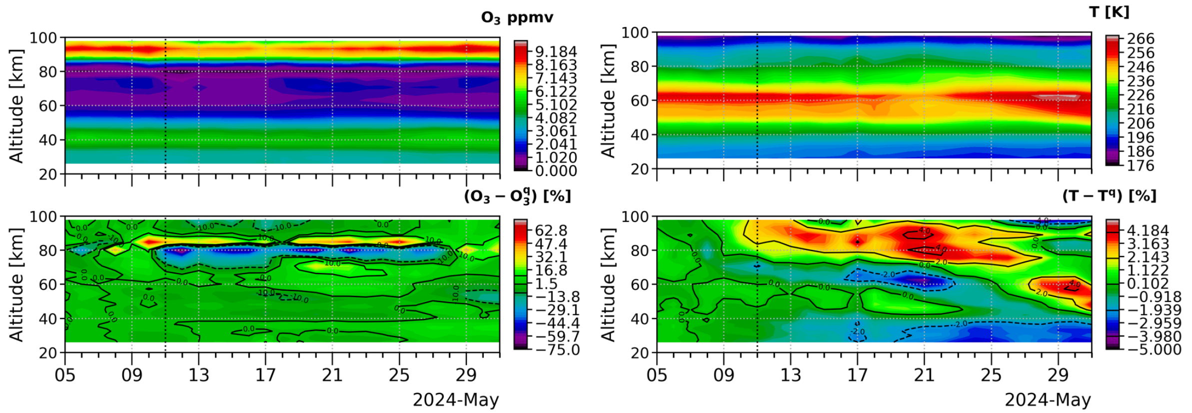

Figure 4. Top left panel: Absolute values of the O_3 vmr measured by the AURA/MLS instrument in the southern hemisphere throughout the month of May 2024. Bottom left panel: Relative difference (in [%]) between the mean quiet condition ozone profiles (O_3^q O_3^q) and the daily ozone profiles from the AURA/MLS instrument, during the whole period between May 05 and May 30 31 (O_3 O_3). Top right panel: Temperature profiles expressed in K. Bottom Right panel: same for temperature Relative difference profiles of the temperature expressed in %. Quiet conditions correspond to the period spanning from May 5 to May 9, 2024. The vertical black line displays the day when the daily Dst index reached its minimal value, indicating the end of the main phase of the geomagnetic storm on May 11 also corresponding to the peak proton flux for the event.

difference profiles observed at this altitude in the middle panel of the figure. Nonetheless, the slightly expanded layer was also impacted by the storm. Similar to the tertiary layer, a smaller depletion is observed by MLS. As for the lower altitudes, the decrease of ozone vmr in the MLT seems to start starts one day before the peak of the storm. However, the ozone loss is relatively small, mainly remaining below 10%. Nonetheless, the ozone depletion reached 20% and 15% on May 13^{th} and 17^{th} respectively corresponding to periods of increased electron precipitation (see Fig. 2 bottom panel). Finally, no significant change in O_3 O_3 vmr has been observed by MLS after the storm of May in the stratosphere.

The bottom panel right panels of Fig. 4 is are the same as the top panel left panels but for the temperature measurements from MLS. The the MLS instrument. The observations of the absolute temperature (top right) show a warming of the atmosphere above 70 km while a clear decrease of temperature can be observed starting on May 17^{th} between 60 km and 50 km. The changes observed during this period are confined between -5% and 5% through the entire altitude range. However, it is apparent in the figure that after the storm and SEP of May $11th$, the entire atmosphere above 75 km heats up while below this altitude, the general trend is a cooling, except from May 27^{th} to the 31^{th} between 45 km and 70 km. It is important to note that the warming of the upper atmosphere starts two days before the event. As for the ozone, this premature atmospheric warming coincides with the early arrival of low energy protons in the atmosphere, as well as an early increase of electron precipitation before the SEP took place. Below 40 km, the temperature constantly decreases from the event onward. However, this change in temperature is caused by the seasonal variability. The heating observed in the upper part of the atmosphere is most likely

~~caused by particle heating and joule heating. A part of the energy of the EPP is lost as heat in the atmosphere and some of its energy is dissipated when they move in the effective electric field of the Earth Sinnhuber et al. (2012).~~

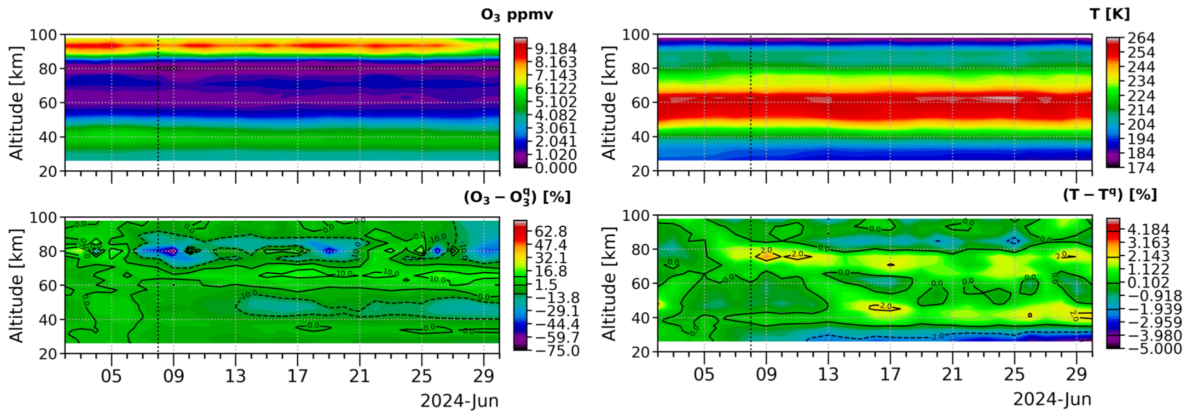

Figure 5. Top left panel: Absolute values of the O_3 vmr measured by the AURA/MLS instrument in the southern hemisphere throughout the month of May 2024. Bottom left panel: Relative difference (in [%]) between the mean quiet condition ozone profiles (~~O_3^q~~ O_3^q) and the daily ozone profiles from the AURA/MLS instrument, during the whole period between June 02 and June 30 (~~O_3~~ O_3). Top right panel: Temperature profiles expressed in K. Bottom Right panel: ~~same for temperature~~ Relative difference profiles of the temperature expressed in %. Quiet conditions correspond to the period spanning from June 02 to June 07, 2024. The vertical black line displays the day of peak proton flux for this event.

The ~~two~~ four panels of Fig. 5 are similar to those of Fig. 4 but for MLS observations just before and after the SEP of June 8^{th}. Again, the ~~top panel shows~~ left panels show the results for ozone. Despite being more intense than in May, this SEP had no influence on the stratospheric ozone. At around 50 km, the ozone vmr gradually decreases from the time of the SEP onward. Below this altitude, no noticeable change was observed by ~~MLS. The slow ozone depletion~~ the MLS instrument. The decrease in ozone at 50 km that start two days before the SEP which remains until the end of June can be explained by long term (seasonal) variations rather than the effect of EPP (see Fig. 1 middle panel). The day following the proton injection of June, AURA/MLS measurements show a depletion of 60% in ozone vmr at 80 km. Although not as intense as at 80 km, the depletion in ~~O_3~~ O_3 vmr occurred between 70 km and 90 km and was of about 20%. In the MLT region, no change in ozone is discernible in the observations.

The ~~bottom panel~~ right panels of the figure ~~shows the relative difference in atmospheric~~ show the results for the temperature. The maximum changes in temperature observed in June are limited between -2% and 2%, which is quite less that in May. As in May, below 40 km, the temperature observations show a steady decrease caused by seasonal variations as winter starts in the SH. Between 40 km and 80 km, the general behavior of the atmosphere is a small warming which is lasting for the whole period as is not likely to be linked ~~to the proton~~ particle precipitation.

4 Discussion and conclusions

In this work, we presented the first observations of the atmospheric ozone response to the extreme geomagnetic storm and SEP that took place on May 11^{th} and June 8^{th} 2024. We mainly used AURA/MLS observations which provided measurements of ozone and temperature profiles at high latitude in both hemispheres~~due to its low Earth orbit~~.

The responses of ozone and temperature to the event of May 11^{th} and June 8^{th} are quite different. For the ozone, this can be seen in both the detrended ozone time series in Fig.3 as well as in the relative difference profiles shown in Fig.4 and Fig.5. Much stronger and longer lasting ozone depletion is observed through the atmosphere in May than in June. However, this is ~~easily~~ explained by the difference in the flux of EPP during the two events. In May, an overlap between energetic solar protons observed by GOES and strongly enhanced electron fluxes from the radiation belts observed by POES have precipitated in the atmosphere. In June, electron precipitation is observed the day before the SEP reached the Earth, but does not continue due to the lack of strong geomagnetic disturbances for this event. For the temperature, after the extreme storm of May, measurements of the MLS instrument show a warming of the atmosphere above 80 km. This is in agreement with the recent study from (Liu et al. (2025)) in which they report a global increase in the temperature of the MLT region during this event with observations performed by the SABER instrument. Conversely in June, we observe a 2% cooling of the atmosphere above 80 km while the atmosphere between 70 and 80 km heats up by 2%. Due to the complexity of the dynamics in the MLT region, the measurements of the MLS instrument alone is not sufficient to determine the physical processes that led the observed heating following the storm of May. Further investigations with a model of the MLT region are required to draw educated conclusions.

Aside the seasonal variations, there is a clear difference in the behavior of ozone in the northern and southern hemisphere after the precipitation of energetic particles in the high latitude atmosphere. During the event of May 11^{th}, MLS observations show a clear decrease of ozone in the southern polar mesosphere. The detrended time series shown in Fig.3 also indicate that the ozone in the secondary layer and tertiary layer decreased simultaneously during the storm of May, which is in agreement with the relative difference profiles presented in Fig.4. However, the detrended time series show that the largest variations in absolute values occurred in the MLT whereas the largest variations observed in the relative differences are observed in the tertiary layer. This is explained by the fact that the absolute values of ozone are lower (around 1.5 ppmv) compared to the secondary layer in which the absolute values of ozone vmr are higher (around 8.5 ppmv). In the northern hemisphere however, only two short lived decreases in ozone took place in the MLT region above 90 km, on May 13^{th} and on the 17^{th}, each of them lasting for two days. These inter-hemispheric differences are strongly linked to the local season. For geomagnetic activity, hence electron precipitation, ~~Mironova et al. (2023)~~ (Mironova et al. (2023)) showed through a one dimensional Radiative-Convective Photochemical model that ozone depletion in the mesosphere ~~were~~ was only possible during local spring, winter and fall, with the strongest one only taking place in winter. Those conclusions also apply for solar protons as shown with MLS observations between 2004 and 2024 by ~~Doronin et al. (2024) and by Xiong et al. (2023)~~ (Doronin et al. (2024)) and by (Xiong et al. (2023)) for the severe SEP of January 2012. In our observations of the June SEP, no significant changes in ~~O_3~~ O_3 were observed in the northern hemisphere whereas a drop of ~~60~~30% occurred at ~~80~~ 75 km in the polar southern hemisphere.

In the MLT regionIn the secondary layer, decreases in ozone are only observed during the event of May 2024. At those altitudes, the maximum decrease in O_3 O_3 is reached two days after the storm unlike in the mesosphere where it is reached in one day. In the MLT region, Jia et al. (2024) this layer (between 90 km and 100 km), (Jia et al. (2024)) have discussed that the decrease in ozone are is not linked to catalytic reactions with HO_x and NO_x HO_x and NO_x, but rather to changes in the mean meridional circulation (MMC) induced by EPP. The perturbed MMC transports $[O]$ and $[H]$ in the polar MLT which, associated to the heating of the thermosphere, can lead to the decrease of ozone concentration. This process may explain the changes of ozone observed after the storm of May which featured a significant caused the heating of the upper atmosphere. Furthermore, in June, no significant heating of the lower thermosphere was observed by MLS and no significant variation of ozone is observed. However, observations of $[O]$ and $[H]$ should be considered to verify this hypothesis.

Finally, measurements from MLS do not show a quick response of stratospheric ozone after the May and June events . In both cases, the spectrum of solar protons was hard enough to produce ionization in the upper stratosphere. In May , no significant change in ozone concentrations is observed any immediate response of ozone to the events of May and June below 60 km. This absence of response in stratospheric ozone could be explained by the season again. Indeed, Denton et al. (2018) have shown in the northern hemisphere with observations of 191 SEPs that ozone depletion following an event was never observed in absence of the polar vortex. Thus, stratospheric depletions are only visible during polar winter, which is not the case in May in the southern hemisphere. In June, ozone is depleted by 10% 5 days after the storm at 50 km. However, this slow persistent decrease in ozone over time is fitting the long term variation of ozone computed with the lowess algorithm. Moreover, even though June marks the winter in the SH, the decrease in ozone concentration observed by MLS is not consistent with a descent of NO_x from high altitudes, as no depletion is observed between 60 km and 70 km. In addition, a direct production of NO_x in the upper stratosphere would cause a decrease of ozone quickly after the storm, which is not observed here.

Data availability. All data are available in the zenodo (Winant et al. (2024)). OMNI data are available at https://omniweb.gsfc.nasa.gov/ow.html, Version 5 of AURA/MLS level 2 data and user recommendations can be found at https://disc.gsfc.nasa.gov/datasets, GOES proton integral fluxes can be found at GOESdataareaccessibleat:https://lasp.colorado.edu/space-weather-portal/, MEPED electron fluxes are accessible at ttps://lasp.colorado.edu/space-weather-portal/

Author contributions. AW made the present analyses and wrote the manuscript with the contribution of the other authors. VP conceptualized and supervised the study, and contributed to the interpretation of the results. All authors contributed to writing of the manuscript through reviews and edits.

Competing interests. The author declare that they have no conflict of interests

Acknowledgements. The project 21GRD02 BIOSPHERE has received funding from the European Partnership on Metrology, co-financed by the European Union's Horizon Europe Research and Innovation Programme and by the Participating States. The authors acknowledge the Horizon 2020 PITHIA-NRF project with Grant Agreement 101007599.

The results presented in this document rely on data provided by the Community Coordinated Modeling Center at Goddard Space Flight Center through their integrated Space Weather Analysis (iSWA) system's HAPI server (https://iswa.gsfc.nasa.gov/IswaSystemWebApp/hapi). The CCMC is a multi-agency partnership between NASA, AFMC, AFOSR, AFRL, AFWA, NOAA, NSF and ONR. These data were accessed via the University of Colorado's Space Weather Technology, Research, and Education Center's (https://colorado.edu/spaceweather) Space Weather Data Portal (https://lasp.colorado.edu/space-weather-portal).

References

Abe, O., Fakomiti, M., Igboama, W., Akinola, O., Ogunmodimu, O., and Migoya-Orué, Y.: Statistical analysis of the occurrence rate of geomagnetic storms during solar cycles 20–24, Advances in Space Research, 71, 2240–2251, 2023.

Andersson, M. E., Verronen, P. T., Wang, S., Rodger, C. J., Clilverd, M. A., and Carson, B. R.: Precipitating radiation belt electrons and enhancements of mesospheric hydroxyl during 2004–2009, Journal of Geophysical Research: Atmospheres, 117, 2012.

Andersson, M. E., Verronen, P. T., Rodger, C. J., Clilverd, M. A., and Seppälä, A.: Missing driver in the Sun–Earth connection from energetic electron precipitation impacts mesospheric ozone, Nature Communications, 5, 5197, https://doi.org/10.1038/ncomms6197, 2014.

Cleveland, W. S.: Robust locally weighted regression and smoothing scatterplots, Journal of the American statistical association, 74, 829–836, 1979.

Denton, M. H., Kivi, R., Ulich, T., Clilverd, M. A., Rodger, C. J., and von der Gathen, P.: Northern hemisphere stratospheric ozone depletion caused by solar proton events: the role of the polar vortex, Geophysical Research Letters, 45, 2115–2124, 2018.

Doronin, G., Mironova, I., Bobrov, N., and Rozanov, E.: Mesospheric Ozone Depletion during 2004–2024 as a Function of Solar Proton Events Intensity, Atmosphere, 15, 944, 2024.

Elvidge, S. and Themens, D. R.: The probability of the May 2024 geomagnetic superstorm, Space Weather, 23, e2024SW004 113, 2025.

Evans, D. and Greer, M.: Polar orbiting environmental satellite space environment monitor, NOAA National Geophysical Data Center, 2000.

Evans, J. S., Correira, J., Lumpe, J. D., Eastes, R. W., Gan, Q., Laskar, F. I., Aryal, S., Wang, W., Burns, A. G., Beland, S., Cai, X., Codrescu, M., England, S., Greer, K., Krywonos, A., McClintock, W. E., Plummer, T., and Veibell, V.: GOLD Observations of the Thermospheric Response to the 10–12 May 2024 Gannon Superstorm, Geophysical Research Letters, 51, e2024GL110 506, https://doi.org/10.1029/2024GL110506, 2024.

Funke, B., López-Puertas, M., Gil-López, S., Von Clarmann, T., Stiller, G. P., Fischer, H., and Kellmann, S.: Downward transport of upper atmospheric NO_x into the polar stratosphere and lower mesosphere during the Antarctic 2003 and Arctic 2002/2003 winters, Journal of Geophysical Research: Atmospheres, 110, 2005JD006 463, https://doi.org/10.1029/2005JD006463, 2005.

Funke, B., López-Puertas, M., Stiller, G., and Von Clarmann, T.: Mesospheric and stratospheric NOy produced by energetic particle precipitation during 2002–2012, Journal of Geophysical Research: Atmospheres, 119, 4429–4446, 2014.

Funke, B., López-Puertas, M., Stiller, G. P., Versick, S., and von Clarmann, T.: A semi-empirical model for mesospheric and stratospheric NO y produced by energetic particle precipitation, Atmospheric Chemistry and Physics, 16, 8667–8693, 2016.

Grenfell, J. L., Lehmann, R., Mieth, P., Langematz, U., and Steil, B.: Chemical reaction pathways affecting stratospheric and mesospheric ozone, Journal of Geophysical Research: Atmospheres, 111, 2004JD005 713, https://doi.org/10.1029/2004JD005713, 2006.

Hayakawa, H., Ebihara, Y., Mishev, A., Koldobskiy, S., Kusano, K., Bechet, S., Yashiro, S., Iwai, K., Shinbori, A., Mursula, K., et al.: The Solar and Geomagnetic Storms in 2024 May: A Flash Data Report, The Astrophysical Journal, 979, 49, 2025.

Huang, F., Lei, J., Zhang, S.-R., Wang, Y., Li, Z., Zhong, J., Yan, R., Aa, E., Zhima, Z., and Luan, X.: Peculiar nighttime ionospheric enhancements over the Asian sector during the May 2024 Superstorm, Journal of Geophysical Research: Space Physics, 129, e2024JA033 350, 2024.

Jackman, C. H., McPeters, R. D., Labow, G. J., Fleming, E. L., Praderas, C. J., and Russell, J. M.: Northern hemisphere atmospheric effects due to the July 2000 Solar Proton Event, Geophysical Research Letters, 28, 2883–2886, https://doi.org/10.1029/2001GL013221, 2001.

Jaswal, P., Sinha, S., and Nandy, D.: Deconstructing the Properties of Solar Super Active Region 13664 in the Context of the Historic Geomagnetic Storm of 2024 May 10–11, The Astrophysical Journal, 979, 31, 2025.

Jia, J., Kero, A., Kalakoski, N., Szeląg, M. E., and Verronen, P. T.: Is there a direct solar proton impact on lower-stratospheric ozone?, Atmospheric Chemistry and Physics, 20, 14 969–14 982, 2020.

Jia, J., Murberg, L. E., Løvset, T., Orsolini, Y. J., Espy, P. J., Zeller, L. C., Salinas, C. C. J. H., Lee, J. N., Wu, D., and Zhang, J.: Energetic particle precipitation influences global secondary ozone distribution, Communications Earth & Environment, 5, 270, 2024.

Kwak, Y.-S., Kim, J.-H., Kim, S., Miyashita, Y., Yang, T., Park, S.-H., Lim, E.-K., Jung, J., Kam, H., Lee, J., et al.: Observational Overview of the May 2024 G5-Level Geomagnetic Storm: From Solar Eruptions to Terrestrial Consequences, Journal of Astronomy and Space Sciences, 41, 171–194, 2024.

Lary, D.: Catalytic destruction of stratospheric ozone, Journal of Geophysical Research: Atmospheres, 102, 21 515–21 526, 1997.

Liu, X., Xu, J., Yue, J., Wang, W., and Moro, J.: Mesosphere and Lower Thermosphere Temperature Responses to the May 2024 Mother's Day Storm, Geophysical Research Letters, 52, e2024GL112 179, https://doi.org/10.1029/2024GL112179, 2025.

Marsh, D., Smith, A., Brasseur, G., Kaufmann, M., and Grossmann, K.: The existence of a tertiary ozone maximum in the high-latitude middle mesosphere, Geophysical Research Letters, 28, 4531–4534, 2001.

Mavromichalaki, H., Papailiou, M.-C., Livada, M., Gerontidou, M., Paschalis, P., Stassinakis, A., Abunina, M., Shlyk, N., Abunin, A., Belov, A., et al.: Unusual Forbush Decreases and Geomagnetic Storms on 24 March, 2024 and 11 May, 2024, Atmosphere, 15, 1033, 2024.

Mironova, I., Aplin, K. L., Arnold, F., Bazilevskaya, G. A., Harrison, R. G., Krivolutsky, A. A., Nicoll, K. A., Rozanov, E. V., Turunen, E., and Usoskin, I. G.: Energetic particle influence on the Earth's atmosphere, Space science reviews, 194, 1–96, 2015.

Mironova, I., Grankin, D., and Rozanov, E.: Mesospheric ozone depletion depending on different levels of geomagnetic disturbances and seasons, Atmosphere, 14, 1205, 2023.

Pickett, H. M., Read, W. G., Lee, K. K., and Yung, Y. L.: Observation of night OH in the mesosphere, Geophysical Research Letters, 33, 2006GL026 910, https://doi.org/10.1029/2006GL026910, 2006.

Pierrard, V., Winant, A., Botek, E., and Péters de Bonhome, M.: The Mother's Day Solar Storm of 11 May 2024 and Its Effect on Earth's Radiation Belts, Universe, 10, 391, 2024.

Randall, C., Harvey, V., Singleton, C., Bailey, S., Bernath, P., Codrescu, M., Nakajima, H., and Russell III, J.: Energetic particle precipitation effects on the Southern Hemisphere stratosphere in 1992–2005, Journal of Geophysical Research: Atmospheres, 112, 2007.

Ranjan, A. K., Nailwal, D., Sunil Krishna, M. V., Kumar, A., and Sarkhel, S.: Evidence of Potential Thermospheric Overcooling During the May 2024 Geomagnetic Superstorm, Journal of Geophysical Research: Space Physics, 129, e2024JA033 148, https://doi.org/10.1029/2024JA033148, 2024.

Rodger, C. J., Clilverd, M. A., Green, J. C., and Lam, M. M.: Use of POES SEM-2 observations to examine radiation belt dynamics and energetic electron precipitation into the atmosphere, Journal of Geophysical Research: Space Physics, 115, 2010.

Rozanov, E., Calisto, M., Egorova, T., Peter, T., and Schmutz, W.: Influence of the precipitating energetic particles on atmospheric chemistry and climate, Surveys in geophysics, 33, 483–501, 2012.

Sætre, C., Stadsnes, J., Nesse, H., Aksnes, A., Petrinec, S., Barth, C., Baker, D., Vondrak, R., and Østgaard, N.: Energetic electron precipitation and the NO abundance in the upper atmosphere: A direct comparison during a geomagnetic storm, Journal of Geophysical Research: Space Physics, 109, 2004.

Sátori, G., Williams, E., Price, C., Boldi, R., Koloskov, A., Yampolski, Y., Guha, A., and Barta, V.: Effects of energetic solar emissions on the Earth–ionosphere cavity of Schumann resonances, Surveys in Geophysics, 37, 757–789, 2016.

Schwartz, M.: MLS/Aura Level 2 Ozone (O3) Mixing Ratio V005, https://doi.org/10.5067/AURA/MLS/DATA2516, 2021.

Seppälä, A., Matthes, K., Randall, C., and Mironova, I.: What is the solar influence on climate? Overview of activities during CAWSES-II. Progress in Earth and Planetary Science, 1, 24, DOI. ADS, 2014.

Seppälä, A., Verronen, P. T., Sofieva, V. F., Tamminen, J., Kyrölä, E., Rodger, C. J., and Clilverd, M. A.: Destruction of the tertiary ozone maximum during a solar proton event, Geophysical Research Letters, 33, 2005GL025 571, https://doi.org/10.1029/2005GL025571, 2006.

Singh, R., Scipión, D. E., Kuyeng, K., Condor, P., De La Jara, C., Velasquez, J. P., Flores, R., and Ivan, E.: Ionospheric disturbances observed over the Peruvian sector during the Mother's Day Storm (G5-level) on 10–12 May 2024, Journal of Geophysical Research: Space Physics, 129, e2024JA033 003, 2024.

Sinnhuber, M., Nieder, H., and Wieters, N.: Energetic particle precipitation and the chemistry of the mesosphere/lower thermosphere, Surveys in Geophysics, 33, 1281–1334, 2012.

Smith, A. K. and Marsh, D. R.: Processes that account for the ozone maximum at the mesopause, Journal of Geophysical Research: Atmospheres, 110, 2005.

Smith, A. K., Espy, P. J., López-Puertas, M., and Tweedy, O. V.: Spatial and temporal structure of the tertiary ozone maximum in the polar winter mesosphere, Journal of Geophysical Research: Atmospheres, 123, 4373–4389, 2018a.

Smith, A. K., Espy, P. J., López-Puertas, M., and Tweedy, O. V.: Spatial and Temporal Structure of the Tertiary Ozone Maximum in the Polar Winter Mesosphere, Journal of Geophysical Research: Atmospheres, 123, 4373–4389, https://doi.org/10.1029/2017JD028030, 2018b.

Sofieva, V. F., Kyrölä, E., Verronen, P. T., Seppälä, A., Tamminen, J., Marsh, D. R., Smith, A. K., Bertaux, J.-L., Hauchecorne, A., Dalaudier, F., Fussen, D., Vanhellemont, F., Fanton d'Andon, O., Barrot, G., Guirlet, M., Fehr, T., and Saavedra, L.: Spatio-temporal observations of the tertiary ozone maximum, Atmospheric Chemistry and Physics, 9, 4439–4445, https://doi.org/10.5194/acp-9-4439-2009, 2009.

Solomon, S., Rusch, D., Gérard, J.-C., Reid, G., and Crutzen, P.: The effect of particle precipitation events on the neutral and ion chemistry of the middle atmosphere: II. Odd hydrogen, Planetary and Space Science, 29, 885–893, 1981.

Solomon, S., Crutzen, P. J., and Roble, R. G.: Photochemical coupling between the thermosphere and the lower atmosphere: 1. Odd nitrogen from 50 to 120 km, Journal of Geophysical Research: Oceans, 87, 7206–7220, https://doi.org/10.1029/JC087iC09p07206, 1982.

Themens, D. R., Elvidge, S., McCaffrey, A., Jayachandran, P., Coster, A., Varney, R. H., Galkin, I., Goodwin, L. V., Watson, C., Maguire, S., et al.: The high latitude ionospheric response to the major May 2024 geomagnetic storm: A synoptic view, Geophysical Research Letters, 51, e2024GL111 677, 2024.

Turunen, E., Verronen, P. T., Seppälä, A., Rodger, C. J., Clilverd, M. A., Tamminen, J., Enell, C.-F., and Ulich, T.: Impact of different energies of precipitating particles on NOx generation in the middle and upper atmosphere during geomagnetic storms, Journal of Atmospheric and Solar-Terrestrial Physics, 71, 1176–1189, https://doi.org/10.1016/j.jastp.2008.07.005, 2009.

Verronen, P. and Lehmann, R.: Analysis and parameterisation of ionic reactions affecting middle atmospheric HO x and NO y during solar proton events, in: Annales Geophysicae, vol. 31, pp. 909–956, Copernicus Publications Göttingen, Germany, 2013.

Verronen, P., Rodger, C. J., Clilverd, M. A., and Wang, S.: First evidence of mesospheric hydroxyl response to electron precipitation from the radiation belts, Journal of Geophysical Research: Atmospheres, 116, 2011.

Verronen, P. T., Seppälä, A., Kyrölä, E., Tamminen, J., Pickett, H. M., and Turunen, E.: Production of odd hydrogen in the mesosphere during the January 2005 solar proton event, Geophysical Research Letters, 33, 2006GL028 115, https://doi.org/10.1029/2006GL028115, 2006.

Winant, A., Pierrard, V., and Botek, E.: Ozone decrease observed in the upper atmosphere following the May 11th 2024 Mother's day solar storm: dataset., https://doi.org/10.5281/ZENODO.14388032, 2024.

Xiong, S., Li, J., Wei, G., Lu, J., Tian, Y., Zhang, X., Fu, S., Sun, M., Li, Z., Zhang, H., et al.: The northern and southern hemispheric asymmetries of mesospheric ozone at high latitudes during the January 2012 solar proton events, Space Weather, 21, e2023SW003 435, 2023.